The Role of Advanced Materials in the Development of Innovative Manufacturing Processes

Carlo Bruni, Marcello Cabibbo, Mohamad El Mehtedi, Archimede Forcellese, Eleonora Santecchia and Stefano Spigarelli

Abstract The present contribution reports on the cutting-edge research activities performed by the authors in the field of innovative manufacturing processes applied to advanced light alloys. These include Friction Stir Welding (FSW), Friction Stir Extrusion (FSE), and Additive Manufacturing (AM). Two new FSW configurations are here introduced and described. A first double-side friction stir welding (DS-FSW), where the welding is performed on both sheet surfaces, one after the other. A second rotating tool FSW (RT-FSW), in which pin is made to rotate around its centerline welding direction, by 0.5 and 1.0 mm. The feasibility of solid-state recycling of a case study, such as an AA1099 machining chips, is exploited using FSE process. In addition, in order to optimize the die design and the process parameters, finite-element (FE) simulation of the process was carried out. The game-changing potential of the metal AM technology is un-veiled through results obtained on light alloys for biomedical applications produced by Powder Bed Fusion (PBF).

C. Bruni · M. Cabibbo (✉) · M. E. Mehtedi · A. Forcellese · S. Spigarelli
Department of Industrial Engineering and Mathematical Sciences (DIISM), Università Politecnica delle Marche, Via Brecce Bianche 12, 60131 Ancona, Italy
e-mail: m.cabibbo@univpm.it

C. Bruni
e-mail: c.bruni@univpm.it

M. E. Mehtedi
e-mail: m.elmehtedi@univpm.it

A. Forcellese
e-mail: a.forcellese@univpm.it

S. Spigarelli
e-mail: s.spigarelli@univpm.it

E. Santecchia
INSTM (UdR Ancona), Department of Materials, Environmental Sciences and Urban Planning (SIMAU), Università Politecnica delle Marche, Via Brecce Bianche 12, 60131 Ancona, Italy
e-mail: e.santecchia@pm.univpm.it

S. Longhi et al. (eds.), *The First Outstanding 50 Years of "Università Politecnica delle Marche"*, https://doi.org/10.1007/978-3-030-32762-0_10

1 Innovative Manufacturing Processes Applied to Light Alloys

In the following three different and promising new approaches to manufacturing processes applied to metallic materials will be described. These three processes start with well-known technological processes that were innovated by applying new methods and/or new starting materials, both in terms of new alloys or new material form. Thus, a friction-stir welding (FSW) with different and innovative layout is here presented; an innovative friction-stir extrusion applied to light-alloy chips is here described; new trends on additive manufacturing (AM) new trends on metal additive manufacturing (AM) of light alloys are here reviewed.

1.1 New Approach and Layout of FSW Applied to Aluminum Alloys

FSW produces a high-quality joint, compared to other conventional fusion welding processes, such as laser welding. In fact, FSW is a welding process particularly suited for joining non-metal materials to metals, especially in those cases where it is not possible by using conventional fusion methods [1, 2]. As for the induced structural modification during welding, the weld zone (usually called the nugget zone, NZ) undergoes a solid-state process promoted by the frictional heat between a rotating tool and the welding metal. A plasticized zone (that is both the nugget and the thermos-mechanically affected zone) is induced to form by the rotating tool. This is further extruded from the leading side (advancing, AS) to the trailing side (retreating, RS) of the tool during its steady translation along the joint line [3]. Another key advantage of the FSW is derived from the lack of need for filler material or shielding gas. The temperature involved is typically some 50–100 °C, which is well below the metal melting point and thus there is no volume change during joining. Moreover, it is generally agreed that FSW, compared to the fusion welding techniques, induces rather low residual stresses after welding. This implies process reduced manufacturing costs [4].

Moreover, FSW generally guarantees better tensile, bend, and fatigue properties than fusion welds. Taking advantages of these positive factors, this process has already been applied to a great variety of aluminum alloys, other than many other metallic materials ([3–7] and references therein). In the case of the aluminum alloys, the FSW technique has found may applications, such as external fuel tank of rockets, stock of railways, bridges [5, 6], to cite but few. Other interesting applications of FSW in the aerospace industry include fuselage, structural parts, cryogenic tanks, etc. [3]. Other interesting applications also include the marine applications (like offshore industry) [3, 7].

The microstructure modifications occurring at the central FSW zone (that is the NZ) most usually consists in dynamic recrystallization resulting in the formation of fine equiaxed grains [8]. Since this recrystallized zone usually reduces the welded alloy mechanical properties, an accurate choice of the process parameters, such rotational speed, welding speed, tilt angle and sinking and of the tool geometry (pin and shoulder geometry and size), is required. With this regard, the welding alloy mechanical properties can be optimized by increasing the pin rotational speed, or by decreasing the welding line progression [8].

One of the major possible drawbacks in using FSW against other fusion welding techniques, refer to the tendency to form oxide layers on the butt surface ("kissing-bond" phenomenon) whose formation is attributed to insufficient plunging of the welding tool during FSW [9], and it is usually responsible of the formation of small geometric discontinuities into the NZ [10].

In this context, the present contribution shows the effect of the process parameters, tool geometry and size on the mechanical properties of FSW joints by using a conventional pin, and a non-conventional pinless tool configurations. The potential advantages offered by the pinless tool configuration can be fully exploited only as thin sheets are welded since, as the thickness increases, the shoulder influence becomes ever more localised to the top sheet surface.

A new FSW approach and methodology is here presented, with the aim of promoting a better joint formability. This consists of carrying out the FSW process on both the sheet surfaces. In this process, the first welding operation is followed by a second welding performed at the plate opposite surface. Such an innovative methodology has been defined by three of the present authors (Cabibbo, Forcellese, Simoncini) as double-side friction stir welding (DS-FSW) [11, 12]. This new FSW methodology has proven to be able to seal the geometric discontinuities, possibly produced by the first welding process, by means of the second welding operation performed at the opposite surface at the same experimental conditions. It resulted that the recrystallized grain structure across the NZ is more homogeneous respect to the surrounding FSW zones, compared to the conventional FSW. Such improvement in the joint quality is very attractive, especially in those cases where the joint materials are meant to be subjected to post-welding forming operations.

A further novel approach to the FSW process (defined by authors as RT-type [13]) is also here reviewed. This new configuration consists on a combination of different plate-to-pin motions. In one configuration, the pin axial spin rotation is set perpendicularly to the sheet blanks travelling along the welding line, with a lateral rotation radius $R = 0$, 0.5, and 1 mm. In a second configuration, the pin translation along the welding plate is set parallel to the welding line.

Both these new welding approaches were compared with the conventional FSW procedures, using the same aluminum alloys.

1.1.1 Description of the New FSW Process Set-Ups

Double-Side FSW (DS-FSW) Method

As for the double-side FSW (DS-FSW) method, a conical pin tool geometry (H13 steel of HRC = 52), with a shoulder diameter equal to 12 mm and cone base diameter and height of the pin of 3.5 and 1.7 mm, respectively, with a pin angle of 30°. A 19-mm-diameter rotating tool was used. All the welding experiments were carried out with a nutting angle equal to 2°.

Two different sheet positions, with respect to the welding tool, were investigated and are here presented:

i. AS-AS, in which the sheet is placed in the AS, at the first FSW operation, and it is maintained in the same side during the following FSW passage at the opposite surface;
ii. AS-RS, in which the sheet, placed in the AS at the first FSW, to be reversed, in the RS, at the second FSW passage at the opposite surface.

The effect of the process parameters on the conventional and the DS-FSW were inferred using homologous rotational speed values $\omega = 1200–2500$ rpm, and same welding speed v = 60 and 100 mm/min. The conventional FSW was carried out using a tool sinking of 0.2 mm, the DS-FSW reached a sinking of 0.15 mm in the first pass and 0.05 mm in the opposite surface. In DS-FSW AS-AS pin-pin the advancing and retreating sides were maintained fixed for both welding procedures; AS-RS pin-pin consists of reversing the advancing side into retreating side, from the first to the second welding procedure. The third and fourth configuration differs from the first two only in the absence of the pin during the second welding process. In the last two (AS-AS, and AS-RS pinless-pinless) the welding process was performed with no pin in both processes. Figure 1 shows a schematic representation of the three DS-FSW configurations used.

Pin Rotation Deviation from Centerline (RT-FSW) Method

For this purpose, a conical pin tools in H13 steel (HRC = 52) with a 2.3 mm pin height, 3.9 mm in diameter at the shoulder, a 30° pin angle, and a shoulder diameter of 15 mm (applying a vertical force of 1.7 kN) was used (Fig. 2).

The welding motion combine two different plate-to-pin mutual motion set-ups:

(i) a pin axial spin rotation sets perpendicular to the sheet blanks, changing the rotation along the plate centerline by a radius equal to R (=0, corresponding to the conventional FSW, 0.5, and 1 mm);
(ii) a pin translation along a direction parallel to the welding centerline line.

The RT-type FSW innovative approach was compared with the conventional T-type (linear welding motion, i.e. for R = 0). In both the RT-type and T-type FSW processes, the stirring action was exerted by the pin tool rotation around its axis;

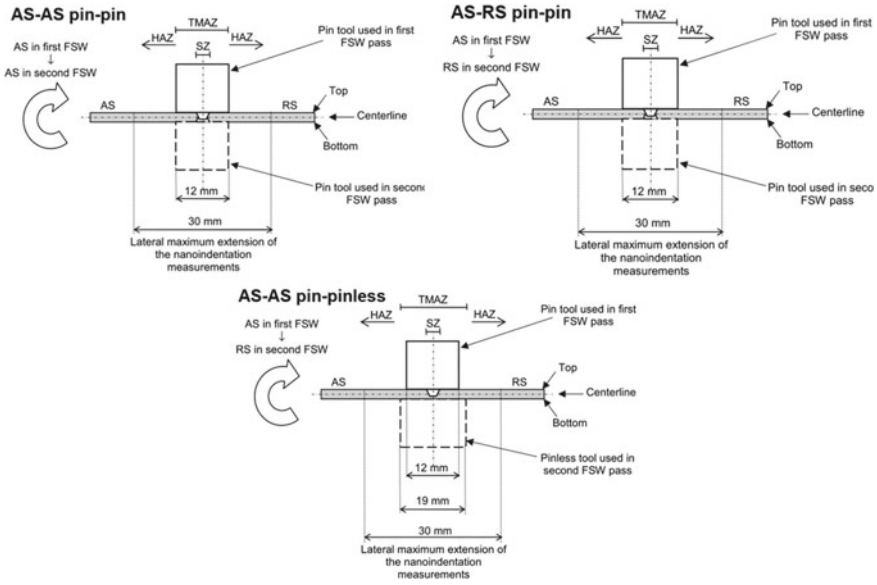

Fig. 1 Representation of the three DS-FSW configurations: AS-AS pin-pin (top left-hand side); AS-RS pin-pin (top right-hand side); AS-AS pin-pinless (bottom)

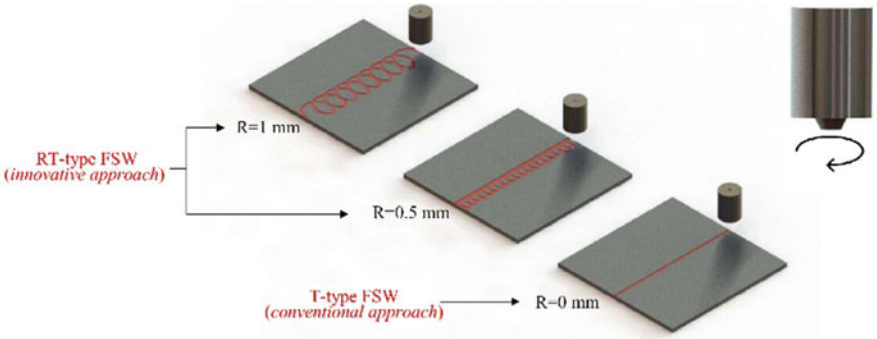

Fig. 2 Conventional (R-type) and T-type FSW configurations

the pin tilt angle was set at 2°, with respect to the normal direction to the plate surface. The RT-type and T-type FSW were performed using a pin rotational speed, $\omega = 2000$ rpm, a transverse speed, $v = 30$ mm/min, and a tool plunging speed of 1.5 mm/min. The above reported setting parameters were chosen by an optimization FSW processing study reported both some of the present authors in [13].

In DS-FSW new approach a heat-treatable AA6082 was used; in the second T-type FSW methodology, a non-heat-treatable AA5754 was welded.

1.2 FSE Applied to Aluminum Chips

Recent literature has revealed some potential variants to the aluminum recycling process compared to the conventional method, therefore without going through the recasting phase, where aluminum alloys are subjected to significant plastic deformations at temperatures below solidus. In 1993, TWI patented a new recycling process to be applied to metal shavings, named Friction Stir Extrusion (FSE).

The process is schematically represented in Fig. 3. This technique belongs to the same family as the Friction Stir Welding technique (FSW) and follows the same principles. It uses the heat generated by friction, between a rotating head and the chips to be recycled, contained within a cylindrical matrix where the head is inserted; the plastic deformation generated by the heat relative to the friction of rotation and the progress of the head involves the mixing, the compaction and the extrusion of the chips. In this way, the FSE process makes it possible to transform the aluminum chips into an extruded product, with high savings in terms of energy, work and economy in relation to the conventional direct extrusion recycling method.

In particular a detectable wires of AA2050 and AA2195 alloys was produced from machining chips by analyzing the amount of heat generated when the head rotation speed varies [14]. Studies have shown how the rotation speed influences the quality of the wires produced in AA7277; high rotational speeds involve hot cracking formation, while low velocity results in cold tearing [15]. Italian researchers have done a campaign on FSE of AA2024 aluminum alloy chips, aimed at the production of MMC within the recycling process by adding SiC powder to the chips [16]. Some of the authors of this research (El Mehtedi, Forcellese, Simoncini, Spigarelli) have studied also how the tool rotation speed affects the extrusion temperature thus influencing the plasticity of the chips [17]. Other researchers focus their studies on recycling of pure Mg chips and AZ31 alloy by means of FSE process [18–21]. A pure aluminum AA1099 was chosen in this study in order to investigate the recycling feasibility of chips and the effect of the process parameters on final properties of the wires. In the early stage, a FE simulation campaign was conducted in order to optimize the die design and the process parameters in terms of plunge rotational speed and

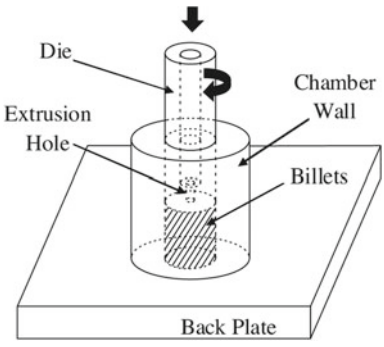

Fig. 3 Synthesis scheme of the FSE process

extrusion rate. The AA1099 aluminum chips were produced by turning of an as-received bar without lubrication. The chips were compacted on a MTS machine. The chip-based billet was FS-extruded at constant rotational speed and plunge rate. The extruded samples were analyzed by optical microscope in order to see the material flow and to characterize the microstructure.

1.2.1 Set-Up Description of Experimental Procedures

The aluminum chips used as extrusion material were produced through machining of AA1099 bar. AA1099 is a pure aluminum with 99.99 of Al (wt.%). The base material is characterized by Ultimate Tensile Strength (UTS) equal to 80 MPa, 38% of elongation and hardness Vickers HV = 22. The machining process was performed without any lubricant or cutting fluid. The approximate dimensions of chips are equal to 8 mm length, 5 width and 0.2 mm thickness.

The chips were compacted in one stroke on a MTS hydraulic universal machine up to 150KN of load (Fig. 4). The resulting chip-billets had a diameter of 40 mm and were 30 mm high. Figure 2 shows the die geometry and the chip-billet after compacting.

The numerical simulation was implemented on the commercial FEM code "SFTC DEFORM 3D", characterized by a Lagrangian implicit solver, in order to design dies and the inserted rotational punch head shown in Fig. 4.

The main components used in the process including a container and a rotating plunger with scroll faced head made of K720 tool steel. The shape of the scrolled face head influences the flow of the plasticized material and affects the final properties. The die is made by a computer numerical control (CNC) milling machine.

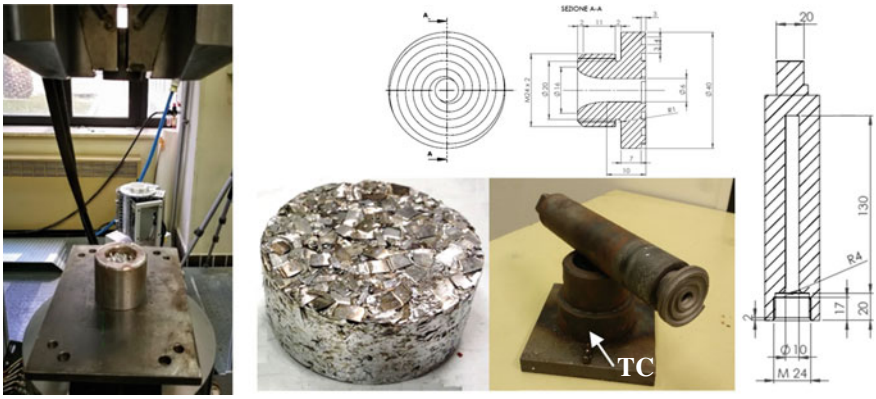

Fig. 4 Compaction machine with a sample of a compacted billet, section of the rotating plunger, front view and section of the inserted rotational punch head and complete set of components for FSE tests

The container cavity is 41 mm in diameter and 70 mm in height. The rotating plunge die has a 40 mm outer diameter with 8 mm central hole which defines the diameter of the extruded wire. The plunger rotates in a clockwise direction and moves toward the container which is charged with Al compacted chips. The rotation and movement of the plunge die relative to the container cause the mixing and stirring of Al chips, during which the contact and pressure between the rotating plunge die and Al chips lead to the conversion of mechanical energy to thermal energy due to the friction. The maximum wire length is limited by geometry of the plunger of 130 mm. Two rotational speeds of 400 and 1000 rpm were implemented under constant plunge rate of 15 mm/min, these values were chosen based on the FEM optimization results. Two k-type thermocouples were used to monitor the temperature changes during the process.

The microstructures of the FSE samples were investigated by optical microscopy (OM) from extruded wire cross-sections cut perpendicular to the extrusion direction.

1.3 Powder Bed Fusion of Ti-Based Light Alloys

Powder bed fusion (PBF), as defined by ASTM 52900:2015, is a widely used AM technique in which a high energy beam sinters or melts the metal powder, layer upon layer, to produce final parts according to a computer-aided design (CAD) model. The near net shape part is built by multiple, rapid heating-melting-solidification cycles, while non-melted powder supports the overall structure until the end of the process. The ability to build complex geometries, not achievable with traditional manufacturing techniques, give unprecedented freedom to designers. Moreover, the high degree of customization achievable makes PBF a great opportunity in wide fields of applications, from automotive and aerospace parts [22] to biomedical prosthesis [23].

If the fusion of the metal powder is performed by an electron beam, the techniques is frequently referred to as electron beam melting (EBM), while in the case of a laser beam the terminologies selective laser melting (SLM) or sintering (SLS), and direct metal laser sintering (DMSL) can be found in literature, according to the degree of fusion of the particles and to the equipment producer. While EBM is performed under vacuum conditions in a heated chamber, laser-based procedures require inert gas atmosphere and the resulting high cooling rates give rise to a finer microstructure [24–26]. These operating conditions reflect in EBM parts that are characterized by a remarkably high surface roughness but are also almost free from residual stresses, while SLM parts show lower surface roughness but high residual stresses, which should be reduced with thermal treatments.

Post-production surface treatments such as laser peening, cavitation peening, or shot peening, are usually performed to meet the surface finishing requirements given by the end-users, and to add local compressive stress to improve cracking resistance and fatigue life [27, 28].

Titanium powder and in particular pre-alloyed Ti-6Al-4V metal powders are among the most studied materials in terms of additive manufacturing [29, 30], owing to excellent mechanical properties (high specific strength and fatigue resistance) coupled with low weight and good biocompatibility. Moreover, the Ti-6Al-4V alloy is the most used titanium alloy for additive manufacturing and covers almost 50% of the overall titanium alloy market.

2 Technological Results and Overview

In the following the experimental results and the technological impacts of the new three innovative manufacturing processes are reported. An overview of the technological impact is also presented. This is intended to promote the here described new promising techniques among the scientific community working in the field of welding of metallic materials, new forming metallic materials from scraps, and the new trends on the AM of Ti-based light alloys.

2.1 DS-FSW and RT-FSW

2.1.1 Results and Overview of the Double-Side Friction Stir Welding Method: DS-FSW

Figure 5 shows the stress-strain curves of FSW joints in AA6082 obtained under different values of the rotational speed and welding speed. The joints ductility is shown to be lower in the NZ, respect to the base metal (BM), irrespective of the welding parameters and process methodology [31]. In general, in terms of both the ultimate values of tensile strength and elongation, the conventional FSW joints show a tensile behaviour better than the one exhibited by the DS-FSWed joints. Actually, the conventional FSW process requires a high sinking value in order to generate the frictional heating allowing the material flow necessary to obtain sound joints. Thus,

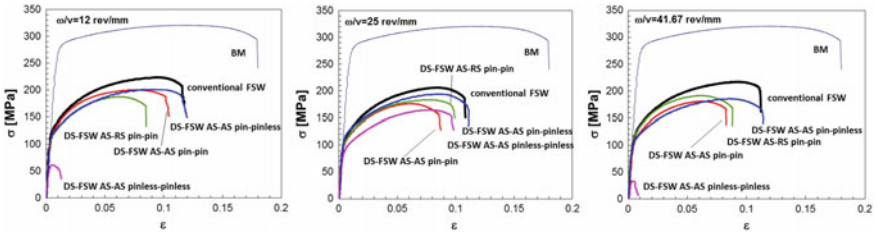

Fig. 5 Tensile stress-strain curves of the DS-FSW, with different welding parameters and tool configurations

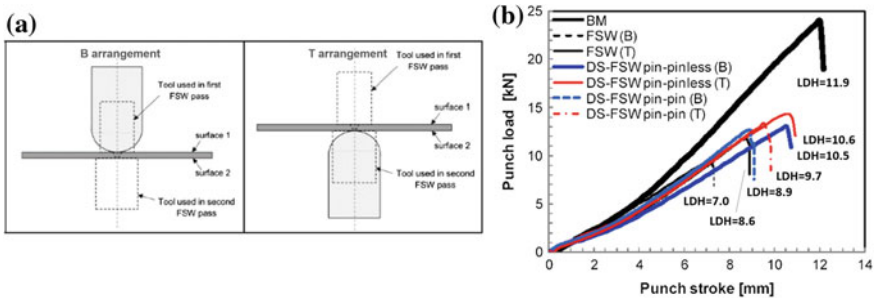

Fig. 6 Hemispherical punch test configurations: in the B arrangement, surface 1 is in contact with the punch, in the T arrangement surface 1 is opposite, (**a**); related test for different experimental conditions (LDH is the Limit Draw Height), (**b**)

in the first pass, by using the same tool sinking as of conventional FSW produces a step in the blank surface that acts as a notch during the second pass. Therefore, the tool sinking value imposed in the second pass had to be further decreased in order to reduce the formation of surface defects. The pinless-pinless configuration has provided the worst tensile properties. In particular, the AS-AS configuration showed low mechanical properties of the joint, while the AS-RS configuration did not reach a sound weldment.

The mechanical behaviour is strongly improved when welding is performed using the pin-pinless configuration. In a recent published work by Cabibbo, Simoncini, Forcellese, the FSW capability to obtain sound joints in 1- and 1.5-mm-thick sheets using a pinless tool was widely documented [12, 31, 32].

LDH (Limit Dome Height) values were lower than those obtained on the BM, no matter what welding methodology was used. Such results reveal that a noticeable formability reduction along the welding zone [10, 12, 31–33]. More specifically, the B arrangement leads to a LDH value lower than the T arrangement (as reported by the letter B, and T, in Fig. 6, and according to the configuration reported in the figure).

In the B arrangement, the local stress field intensity rise, caused by the notch, is responsible of the FSW sample failure at the geometric discontinuity. In the T arrangement, the failure of the deformed joint occurs at the step produced by the sinking action applied by the shoulder [11]. This is mainly due to the biaxial tensile stress state to which the notch is subjected. This appeared to be less severe in the T arrangements, respect to that in the B arrangement.

The DS-FSW joints showed LDH values higher than those measured on the conventional FSW joints. This second welding induces a dual beneficial effect: it allows both the closure of the geometric discontinuity, and the reduction in the height of the step produced by the first welding on the opposite plate surface. Furthermore, the DS-FSW is characterised by uniform recrystallized grains across the NZ, and partially across the thermos-mechanical affected zone (TMAZ), than in the case of the conventional FSW [11]. Finally, the joints obtained using the pin-pinless tool

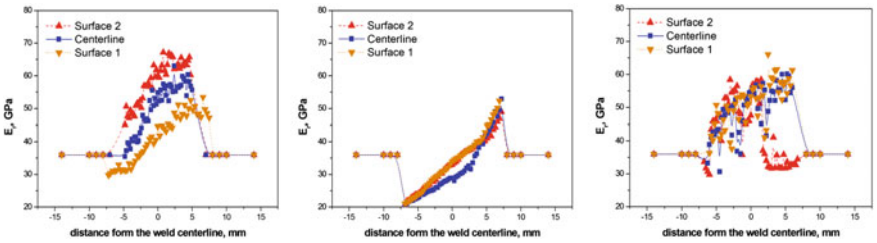

Fig. 7 Nanoindentation E_r profiles of the different used FSW configurations

Table 1 AA6082 DS-FSW mean grain size; the BM SZ had a mean grain size of 20 ± 2 μm

FSW configuration	Mean grain size (μm)				
	AS/TMAZ	Surface 1/SZ	Middle/SZ	Surface 2/SZ	RS/TMAZ
Conventional FSW	14 ± 2	7.8 ± 0.3	7.6 ± 0.3	6.9 ± 0.3	14 ± 2
Pin-pin DS-FSW	12 ± 2	6.3 ± 0.2	6.2 ± 0.2	6.4 ± 0.2	13 ± 2
Pin-pinless DS-FSW	12 ± 2	5.7 ± 0.2	5.7 ± 0.2	5.8 ± 0.2	13 ± 2

configuration lead to LDH values higher than the ones obtained by using the pin-pin configuration, irrespective of the sheets arrangement.

Both the aspects are also confirmed by the nanoindentation inspections on the reduced elastic modulus Er profiles taken across the FSW joints (Fig. 7), and by the corresponding mean grain size analysis carried out by polarized optical microscopy (POM) (Table 1).

The better formability of the DS-FSW, respect to the conventional FSW, is most likely related to the local elastic modulus uniformity (i.e. the reduced Young's modulus) across the weld, and to the less dramatic hardness variation, from top to bottom of the sheet section. In all the three DS-FSW configurations here described, the observed grain size uniformity and morphology across the SZ, from surface to surface, greatly favoured the soundness and better post-welding response of the welded Al-sheets.

2.1.2 Results and Overview of the Friction Stir Welding Method by Pin Rotation Deviation from Centerline: RT-FSW

The AA5754 was subjected to an annealing treatment at 415 °C/3 h followed by furnace cooling, in one case prior FSW (AA5754-O state), and in another case, after FSW (post-weld annealing: PWA) (Fig. 8).

It appeared that the closest mechanical response to the un-welded annealed AA5754 sheet is obtained by welding with R = 0.5 mm in the PWA condition, where UTS differed only by 5%, and ductility differed by 30% respect to the un-welded annealed condition. In the other conditions, the UTS remained within a range

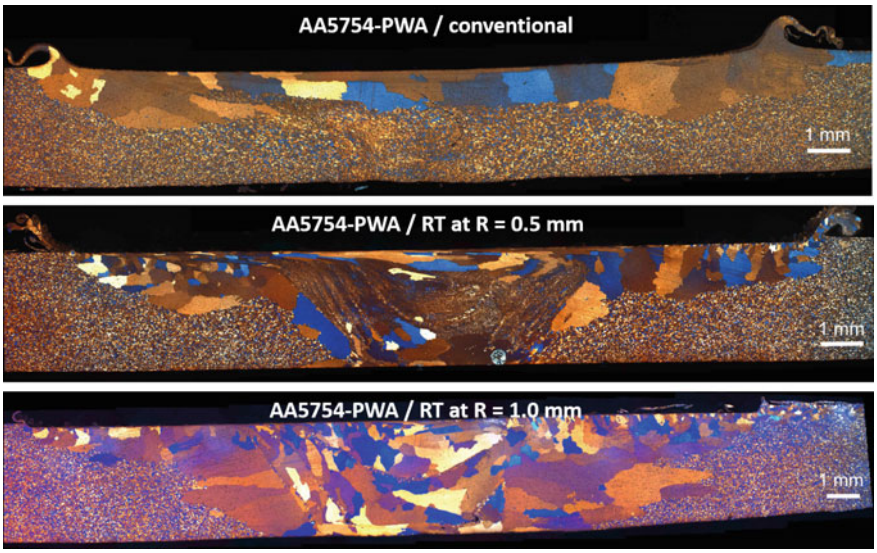

Fig. 8 POM RT-FSW PWA at R = 0 (conventional FSW), 0.5, and 1 mm

of 14% of difference, respect to the annealed sheet, with a ductility reduction ranging from 76 to 30% (Fig. 9).

Thus, based on the microstructure evidence, and the obtained hardness and mechanical response, the use of a RT-type welding motion is justified when the plate is homogenized prior, or, even better, after FSW. Conversely, there is no need to deviate the pin, from its welding centerline, in the case of not-annealed AA5000 FSW.

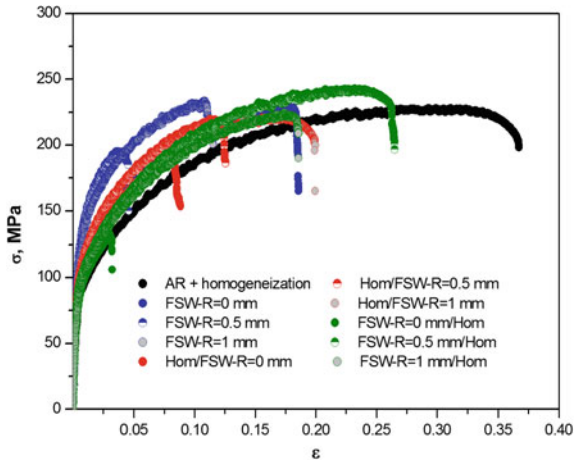

Fig. 9 Tensile stress-strain curves for RT-FSW, in the AA5754-O stare and in the PWA condition, at R = 0 (conventional FSW), 0.5, and 1 mm

2.2 FSE

2.2.1 Results and Overview of FSE Experimental Process

Since it is worth knowing that higher temperature assures better solid bonding between the chips, in order to guarantee extrusion temperatures greater than 400 °C, rotation speed of 1000 rpm were considered.

In fact, in the FSE process, the tool rotation speed affects the extrusion temperature. Figure 10 shows the maximum temperature registered during FSE at different rotation speeds.

The temperatures and the material flow obtained in FE simulations were confirmed by experiments as shown in Fig. 11.

Thanks to the simulations, it was also possible to evaluate the load trend that the CNC machine maintains during the process. Figure 12 shows the presence of a transitional stage lasting about 2 s, in which a sudden increase in the load up to values higher than 90 kN occurs and then an immediate lowering to constant values

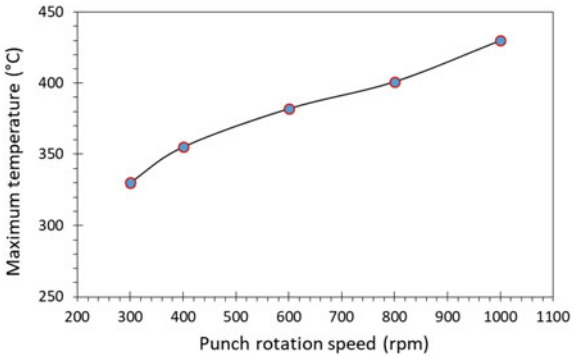

Fig. 10 Maximum temperatures reached at various rotation speed

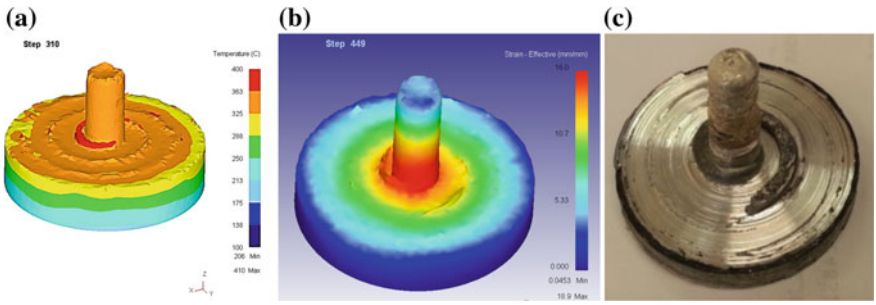

Fig. 11 Temperature and strain distribution during FSE from FEM simulation (**a**), (**b**) and sample obtained experimentally at 1000 rpm (**c**)

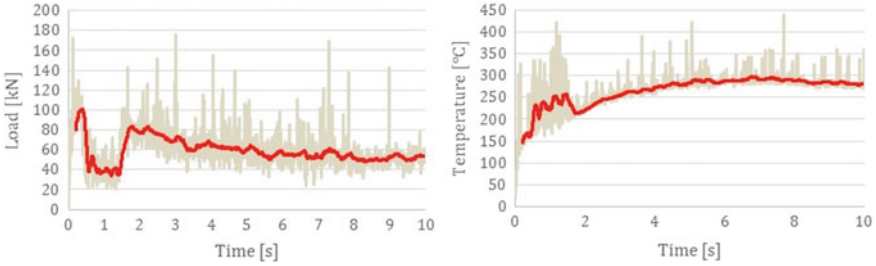

Fig. 12 Load prediction for the CNC machine and max temperature reached during the process

around 40 kN, evidently depending on the first contact between the rotating head and the billet, where the first chip re-meshing takes place.

Therefore, for the seconds part of the test, after the transitional stage, the load is increasing again up to 80 kN due to the low extrusion temperature. In the second stage, the extrusion load decreased slowly by increasing the chips temperature up to a constant a steady state value of 50 kN, as shown in Fig. 12.

The analysis carried out subsequently took place through the OM. In particular, the specimen was observed on the section of the obtained wire and on the section along the vertical plane. In Fig. 13 it is possible to observe the plans that have been analyzed in the OM. The metallography shows mainly the total lack of a homogeneous and uniform structure for the extruded product.

In fact, a set of undefined microstructures was obtained from the tests, with the presence of grains of varying sizes, and above all with defects sometimes not classifiable, accentuated by the presence of real holes (visible with the naked eye on the

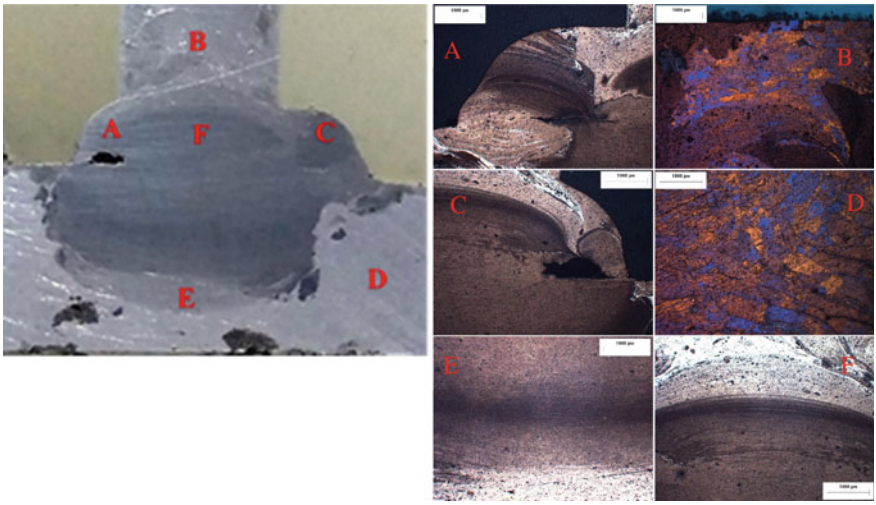

Fig. 13 Section of the residual tablet and metallography at different locations

surface and therefore perfectly framed by optical microscopy). All this is obviously linked to the lack of compaction of the plastic material during extrusion, caused by many factors already analyzed, such as the centrifugal effect due to the high rotation speeds and the not perfect adaptation of the head channels to the processing conditions. However, it is possible to identify the flow of the material quite easily, leaving an indelible trace in its movement from the outside towards the inside of the tablet, conditioned by the rotation of the head on the upper surface.

Moreover, it is possible to observe in Fig. 6, a substantial difference in the morphology of the material remained "trapped" inside the residual tablet between the center and the sides; in the center, as also confirmed by the metallography, the aluminum chips were completely bonded with a very fine microstructure. Whereas, the chips boundary is still visible in the stirred zone far from the center extrusion hole (Fig. 6d).

2.3 Properties of Ti-Based Light Alloys Produced by PBF

Given the intrinsic differences between electron- and laser-based PBF processes, the same as-built (namely with no further post-processing treatment) sample of Ti-6Al-4V will be characterized by a higher surface roughness and a lower fatigue strength if produced by electron beam melting [34]. In terms of comparison between traditional manufacturing techniques and metal additive manufacturing, the performance of samples after post-processing treatments for stress relieve and machining, show a fatigue strength that is comparable or even better than traditional ones [35].

Strong efforts are currently performed by the scientific community to improve parts quality (i.e. density, finishing), and also to optimize the PBF parameters in order to control the microstructure. Moreover, to improve the performance of PBF parts and to widen the range of materials that can be manufactured by PBF techniques, Ti-based light alloys with new formulation tailored for additive manufacturing are under development. Results show that the epitaxial growth typical of additively manufactured titanium alloys can be hindered adding boron to powder blends of Ti-6Al-4V, Ti-12Mo, Ti-20V, due to the grain refinement effect linked to the TiB needles formation [36]. The iron addition to a β-Ti alloy in order to get the Ti-1Al-8V-5Fe formulation (also known as Ti-185), has been investigated by Azizi et al. [37] as feedstock material for selective laser melting. The final AM part produced with the Ti-185 powder show a fine microstructure characterized by the presence of nano-scale α phase inside the β matrix, coupled with high dislocation density. As a result, these peculiar features are responsible for remarkable mechanical properties in terms of strength and plasticity.

New formulations of peritectic titanium alloys with the addition of rare earth elements (i.e., La) have been recently proposed by Barriobero-Vila et al. [38], namely Ti + 2 wt.% La and Ti-1.4Fe-1La (wt.%). The microstructural characterization shows that the resulting orientation of the alpha phase is not always related to that of the beta phase, which reflects in a reduction of texture and equiaxed microstructure.

3 General Considerations and Outlook

Two novel approaches and methodologies of friction stir welding on aluminum alloys were presented. The first approach consists in a double-side FSW (DS-FSW). The second approach is represented by a radial deviation of the rotating pin from its centerline, during FSW (RT-FSW). With respect to conventional FSW, DS-FSW shows more uniform elastic modulus across the sheet section, with respect to the FSW, better formability and higher FLC response. On the other hand, the RT-FSW in post-weld annealing (PWA) condition showed the best mechanical response respect to the un-welded annealed AA5754 sheet.

The feasibility of solid-state recycling of pure aluminum AA1099 chips was investigated using the innovative FSE process to produce defect-free wires. A finite element simulation was initially carried out in order to optimize both the design of the main and secondary components used in the experimental tests. The main results obtained can be summarized as follows: i. excluding the initial transient phase, the temperature greatly influences the extrusion load during the process; as the temperature increases, the machine load progressively decreases until a steady state value. ii. FSE process applied to recycle AA1099 chips allows to obtain wires manufactured with good surface quality, but with non-homogeneous microstructure and with presence of small internal voids.

Titanium based light alloys produced by electron or laser powder bed fusion, are now widely known in the field of metal additive manufacturing. The powerful option of a design which is free from the limitations typical of traditional manufacturing techniques, is strengthened by microstructural and mechanical properties which can be properly customized to be competitive with cast, forged or wrought alloys. The fast growth of the AM technology coupled with the development of new alloys formulations tailored for specific applications or to overcome microstructural weaknesses typical of AM, enlighten the new era of metallurgy.

References

1. Su J-Q, Nelson TW, Mishra R et al (2003) Microstructural investigation of friction stir welded 7050–T651 aluminium. Acta Mater 51:713–729
2. Seidel TU, Reynolds AP (2001) Visualization of the material flow in AA2195 friction-stir welds using a marker insert technique. Metall Mater Trans A 32:2879–2884
3. Nicholas ED, Thomas WM (1998) A review of friction processes for aerospace applications. Int J Mater Prod Technol 13:45–54
4. Dawes CJ, Thomas WM (1996) Friction stir process welds aluminum alloys. Weld J 75:41–45
5. Heinz B, Skrotzki B (2002) Characterization of a friction-stir-welded aluminum alloy 6013. Metall Mater Trans B 33:489–498
6. Mahoney MW, Rhodes CG, Flintoff JG et al (1998) The rate-controlling mechanism in superplasticity. Metall Mater Trans A 29:1955–1964
7. Jata KV, Sankaran KK, Ruschau JJ (2000) Friction-stir welding effects on microstructure and fatigue of aluminum alloy 7050–T7451. Metall Mater Trans A 31:2181–2192

8. Kumbhar NT, Sahoo SK, Samajdar I et al (2011) Microstructure and microtextural studies of friction stir welded aluminium alloy 5052. Mater Des 32:1657–1666
9. Oosterkamp A, Oosterkamp LD, Nordeide A (2004) Kissing bond phenomena in solid-state welds of aluminum alloys. Weld J 83:225s–231s
10. Forcellese A, Fratini L, Gabrielli F et al (2010) Formability of friction stir welded AZ31 magnesium alloy sheets. Mater Sci Forum 638–642:1249–1254
11. Simoncini M, Cabibbo M, Forcellese A (2015) Development of double-side friction stir welding to improve post-welding formability of joints in AA6082 aluminum alloys. Proc IMechE Part B: J Eng Manuf 2015:1–11
12. Cabibbo M, Forcellese A, El Mehtedi M et al (2014) Double side friction stir welding of AA6082 sheets: microstructure and nanoindentation characterization. Mater Sci Eng A 590:209–217
13. Cabibbo M, Forcellese A, Simoncini M et al (2016) Effect of welding motion and pre-/post-annealing of friction stir welded AA5754 joints. Mater Des 93:146–159
14. Tang W, Reynolds AP (2010) Production of wire via friction extrusion of aluminum alloy machining chips. J Mater Process Tech 210:2231–2237
15. Behnagh RA, Mahdavinejad R, Yavari A et al (2014) Production of wire from AA7277 aluminum chips via friction-stir extrusion (FSE). Metall Mater Trans B 45:1484–1489
16. Baffari D, Buffa G, Campanella D et al (2017) Al-SiC Metal matrix composite production through friction stir extrusion of aluminum chips. Proc Eng 207:419–427
17. Mehtedi ME, Forcellese A, Simoncini M et al (2018) A sustainable solid state recycling of pure aluminum by means of friction stir extrusion process (FSE). AIP Conf Proc 1960:030004
18. Behnagh RA, Shen N, Ansari MA et al (2016) Experimental analysis and microstructure modeling of friction stir extrusion of magnesium chips. J Manuf Sci Eng 138:04100
19. Hosseini A, Azarsa E, Davoodi B et al (2012) Effect of process parameters on the physical properties of wires produced by friction extrusion method. Int J Adv Eng. Technol 3:592–597
20. Sharifzadeh M, Ansari MA, Narvan M et al (2015) Evaluation of wear and corrosion resistance of pure Mg wire produced by friction stir extrusion. Trans Nonferrous Metal Soc 25:1847–1855
21. Baffari D, Buffa G, Campanella D et al (2017) Process mechanics in friction stir extrusion of magnesium alloys chips through experiments and numerical simulation. J Manuf Process 29:41–49
22. Dehoff RR, Tallman C, Duty EC (2013) Case study: additive manufacturing of aerospace brackets. Adv Mater Process 171:19–22
23. Frazier WE (2014) Metal additive manufacturing: a review. J Mater Eng Perform 23:1917–1928
24. Kirka MM, Nandwana P, Lee Y et al (2017) Solidification and solid-state transformation sciences in metal additive manufacturing. Scr Mater 135:130–134
25. Murr LE (2018) A metallographic review of 3D printing/additive manufacturing of metal and alloy products and components. Metallogr Microstruct Anal 7:103–132
26. Seifi M, Salem A, Satko D et al (2017) Defect distribution and microstructure heterogeneity effects on fracture resistance and fatigue behavior of EBM Ti–6Al–4V. Int J Fatigue 94:263–287
27. Hackel L, Rankin JR, Rubenchik A et al (2018) Laser peening: a tool for additive manufacturing post-processing. Addit Manuf 24:67–75
28. Sato M, Takakuwa O, Nakai M et al (2016) Using cavitation peening to improve the fatigue life of titanium alloy Ti-6Al-4V manufactured by electron beam melting. Mater Sci Appl 7:181–191
29. Yap CY, Chua CK, Dong ZL et al (2015) Review of selective laser melting: materials and applications. Appl Phys Rev 2:041101
30. Mengucci P, Gatto A, Bassoli E et al (2017) Effects of build orientation and element partitioning on microstructure and mechanical properties of biomedical Ti-6Al-4V alloy produced by laser sintering. J Mech Behav Biomed Mater 71:1–9
31. Simoncini M, Forcellese A (2012) Effect of the welding parameters and tool configuration on micro- and macro-mechanical properties of similar and dissimilar FSWed joints in AA5754 and AZ31 thin sheets. Mater Des 41:50–60

32. Forcellese A, Simoncini M (2012) Plastic flow behaviour and formability of friction stir welded joints in AZ31 thin sheets obtained using the 'pinless' tool configuration. Mater Des 36:123–129
33. Kim D, Lee W, Kim J et al (2010) Formability evaluation of friction stir welded 6111–T4 sheet with respect to joining material direction. Int J Mech Sci 52:612–625
34. Nicoletto G, Konečná R, Frkáň M et al (2018) Surface roughness and directional fatigue behavior of as-built EBM and DMLS Ti6Al4V. Int J Fatigue 116:140–148
35. Beretta S, Romano S et al (2017) A comparison of fatigue strength sensitivity to defects for materials manufactured by AM or traditional processes. Int J Fatigue 94:178–191
36. Mantri SA, Alam T, Choudhuri D et al (2017) The effect of boron on the grain size and texture in additively manufactured β-Ti alloys. J Mater Sci 52:12455–12466
37. Azizi H, Zurob H, Bose B et al (2018) Additive manufacturing of a novel Ti-Al-V-Fe alloy using selective laser melting. Addit Manuf 21:529–535
38. Barriobero-Vila P, Gussone J, Stark A et al (2018) Peritectic titanium alloys for 3D printing. Nat Commun 9:3426